Intensifying process of polarization effect within pixellated CdZnTe detectors for X-ray imaging

Xi Wang (王 玺)[1*], Shali Xiao (肖沙里)[1], Miao Li (黎 森)[1], Liuqiang Zhang (张流强)[1], Yulin Cao (曹玉琳)[2], and Yuxiao Chen (陈宇晓)[2]

[1]*Key Laboratory of Optoelectronic Technology and Systems, Ministry of Education, Chongqing University, Chongqing 400030, China*

[2]*Institute of Electronic Engineering, China Academy of Engineering Physics, Mianyang 621900, China*

[*]*Corresponding author: wangxi20032547@163.com*

Received January 7, 2011; accepted February 21, 2011; posted online May 18, 2011

The intensifying process of polarization effect at room temperature in a pixellated Cadmium zinc telluride (CdZnTe) monolithic detector is studied. The process is attributed to the increase in build up space charges in the CdZnTe crystal, which causes an expansion of the space charge region under the irradiated area. The simulations of electric potential distributions indicate that the distorted electric potential due to the high X-ray flux is significantly changed and even deteriorated due to increasing space charges within the irradiated volume. An agreement between the space charge distribution and electric potential is discussed.

OCIS codes: 040.1880, 160.6000, 230.0040, 340.7440.

doi: 10.3788/COL201109.070401.

Recent developments in laser technology have made it possible to enhance energy on the target through inertial confinement fusion[1]. Therefore, with the increase in energy of lasers for fusion, hard X-ray above 10 keV containing the information of plasma can be detected[2,3]. Cadmium zinc telluride (CdZnTe) is a wide bandgap semiconductor material that has been studied extensively for use as X-ray and γ-ray detectors. One of the most important advantages of nuclear radiation CdZnTe detectors is their ability to operate at room temperature, while offering high detection efficiency and excellent energy resolution. Moreover, the CdZnTe detector is well suited for X-rays between 10 keV and 1 MeV[4]. However, the operation of CdZnTe detectors in high flux X-ray beams can cause detector polarization[5]. In recent years, several reports have discussed the CdZnTe detector polarization aimed at reducing this effect[6−9]. However, little attention has been devoted to the intensifying process of polarization at room temperature.

In this letter, we describe an expanding phenomenon of polarization observed in monolithic CdZnTe devices under increasing high flux X-ray irradiation at room temperature. Furthermore, we present the progression of electric potential distributions with increasing high X-ray flux. The progression reflects the development of build up charge distributions when the device is operated under conditions of high intensity X-ray flux irradiation. The phenomenon is of particular interest for potential applications of CdZnTe detectors in high flux X-ray conditions, such as in the Shenguang III prototype laser facilities or synchrotron radiation.

The 16×16 pixels array detector studied in this letter was fabricated from a 30×30×5 (mm) CdZnTe single crystals grown by the modified vertical Bridgman technique. The cathode contact used was a thermally evaporated indium in a planar configuration, whereas the anode was a thermally evaporated indium with 1.2×1.2 (mm) area pixels forming a 16×16 array on a 1.86-mm pitch. The pixel array was surrounded by a 0.1-mm-thick guard electrode to eliminate possible side-surface leakage current and electric-field distortion effects.

The measurement system consisted of an X-ray source capable of up to 500 μA at 80 kVp. For this system, the majority of X-rays produced by the tube were approximately 25 keV with a maximum energy of 80 keV. The X-ray beam was collimated to the central area of the detector in order to avoid edge pixels. The reason for this is that the edge pixels usually deteriorate and degrade detection performance. In addition, the detector is side shielded to prevent scatter events. In this letter, we considered a detector with a thickness L=5 mm biased at V=−800 V. Its top cathode electrode was exposed to a uniform flux of X-rays passing through a circular collimator of radius R=12.5 mm (Fig. 1). The electronics threshold was set at 5 keV to improve signal-to-noise ratio. A detailed description of the detectors and measurement system can be found in Ref. [10].

Pixel count is considered a function of tube current for a typical non-polarizing detector; thus, the X-ray could be considered a proportion function of the tube current[7]. The set of measurements reported 16×16 pixels detector responses with variable X-ray flux (tube current). Considering the large size of the pixel, all data in Fig. 2 have been interpolated linearly for smoothing. The series of maps in Fig. 2 show the intensity distribution of the polarizing detector irradiated with an increasing high intensity X-ray flux through the circular collimator.

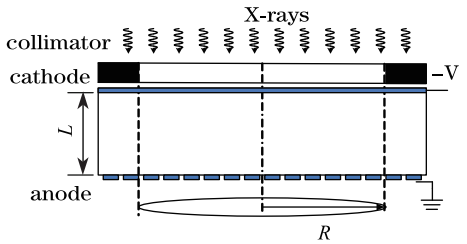

Fig. 1. Experimental setup with uniform X-ray irradiation and circular collimator of a pixellated CdZnTe detector.

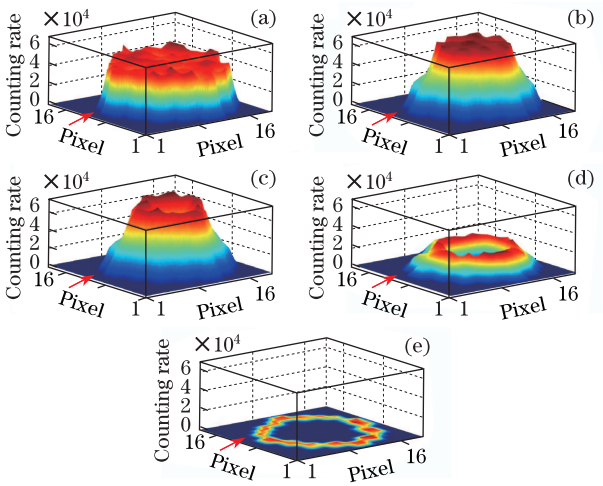

Fig. 2. (Color online) A series of count maps for polarized detector. The detector is irradiated biased at −800 V through a circular collimator of radius R=12.5 mm with increasing flux rates (tube current). Tube voltage is 75 kV, and the currents are (a) 200, (b) 300, (c) 350, (d) 400, and (e) 500 μA, respectively.

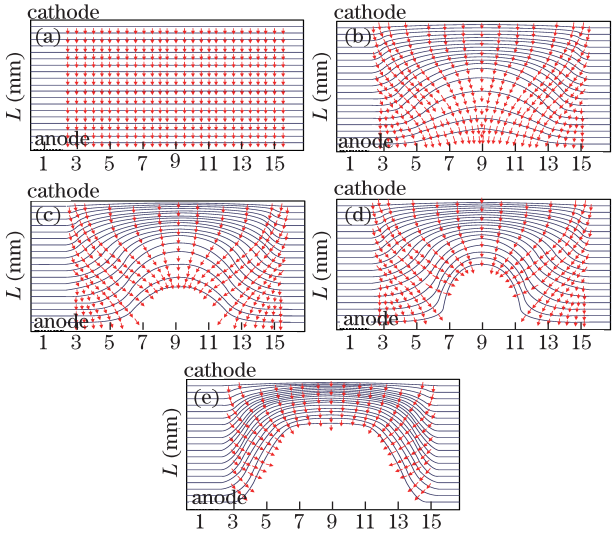

Fig. 3. (Color online) Electric potential lines are shown as blue solid lines with red arrows depicting electron trajectories for part of a 5-mm detector, biased at −800 V and subjected to the increasing flux of photons through a 4-mm diameter collimator. Each plot corresponds to the maps in Fig. 2.

Under low intensity flux X-ray, the detector counted uniformly in the irradiated area and its counting behavior is shown in Fig. 2(a). These results indicate that the pixel counts are proportional to flux. As the X-ray flux increased, the outer irradiated pixels lost counts, whereas the interior ones had some extra counts (Fig. 2(b)). The center pixels lost their counts for too much intensity (Fig. 2(c)). This transition is important in the polarization progression. After further increasing the X-ray flux, the center pixels lose much more counts. Meanwhile, some central pixels appear to have no counts (Fig. 2(d)). Furthermore, all pixels lose counts drastically. The decreasing trend also strengthened as the non-counting area expanded. The total counts of all the pixels decreased greatly, leaving very few counts (Fig. 2(e)). Figures 2(b)−(e) clearly visualize the intensifying process of polarization. In particular, Fig. 2(e) shows that the device nearly shut off at ultra-high X-ray flux, thereby exhibiting a donut-shaped low-counting response pattern.

Generally, the analysis of charge induction within single-polarity detectors designed with general multi-element electrode geometries involves a large matrix of three-dimensional numerical simulations to solve for the electrostatic and weighting fields[11]. However, that method is computationally expensive. Therefore, we utilized a simple, approximate, and analytical method for the weighting potential and charge induction within a pixellated detector. Following our work[12], the electric potential distributions with increasing flux were simulated with the negligible gap width between pixels. Although the simulation results are approximate, they are consistent with the experimental data.

Figure 3 shows the electric potential distributions for the pixellated detector under variable X-ray flux. The fluxes are subjected to the same five increasing ones shown in Fig. 2. These plots are corresponding to the centerline count profiles across the device marked red arrows in the maps of Fig. 2. From these plots, it is obvious that the linear potential due to the bias voltage has been modified significantly by the presence of the space charge within the volume irradiated by the X-ray. These plots provide a possible way of explaining the observed expanding phenomenon of polarization.

In Fig. 3, the blue solid lines show the electric potential contour, and the red arrows represent the equivalent trajectory of electrons. The top is the cathode, and the bottom is the anode marked pixel number in each plot of Fig. 3.

Figure 3(a) shows that the electric potential is uniformly distributed between the cathode (top) and the anode (bottom) at low flux. It is difficult to find the influence of space charges on the electric potential distribution generated by the applied bias. The photo-generated electrons throughout the detector volume can travel in approximately straight lines (cross the equipotential line) as the arrows show. Therefore, in the uniform irradiated area restricted to the circular collimator, the counting pixels can be considered as indiscrimination (Fig. 2(a)).

Meanwhile, Fig. 3(b) shows the potential distribution profiles at an increased flux. In this condition, there is sufficient space charge to create an obvious polarization effect. The profiles clearly show that the electric potential is no longer distributed uniformly between the cathode and the anode, which is consistent with a certain concentration of space charge. The distorted potential contours have a lateral component toward the center. The trajectories of electrons seem to focus on the middle pixels. Therefore, the central pixels get more counts than the outer adjacent ones, and the pixels at the edge of the irradiated region lose counts (Fig. 2(b)).

When the flux is increased, the buildup charges cause the internal potential distribution to deteriorate over the entire volume of the crystal (Fig. 3(c)). There is a small blank region without potential contours at the bottom of the plot, indicating that there are space charges in the region. Moreover, the density of these charges is so high

that potential contours are modified. Therefore, some pixels in the center cannot record too many pulses while the neighboring ones get some extra counts, although it is unnoticeable due to the blend trajectories.

When the flux is increased continually, the blank region expands due to the increased space charges. Thus, there are no trajectories traversing this region for electrons, and the electrons cannot reach the central pixels (Fig. 3(d)). At this high flux, the central pixels shut off completely, and the overall counting rate of all pixels is dramatically reduced. Thus, the shut off pixels appear to be the subsided area in Fig. 2(d).

Finally, once the flux is increased further, the region with buildup charges occupies a great part of plot (Fig. 3(e)). The region not only extends to the cathode (top) but also to the lateral sides. The lateral component of electric potential contour is greatly increased. Hence, there are no electron trajectories towards the interior irradiated pixels, and most of the interior pixels are shut off completely. In addition, the subsided area expands and only the pixels near the irradiated edge can continue counting while others have been shut off (Fig. 2(e)).

A modification of the internal field profile is found in CdZnTe under conditions of high charge injection due to high photon flux. The net effective field across the device is collapsed and intensified due to the development of build up charge. This behavior is consistent with the build up of positive space charges caused by photogenerated holes. Indeed, at high flux irradiation, the rate of charge injection into the CdZnTe is sufficiently high such that charge trapping dominates over thermal emission and recombination processes, and a significant net space charge accumulates in the bulk. Originally, a region with high density of space charges is present in center of irradiation area and there are no trajectories to anode pixels for electrons. And then, the region expanded to the edge as the build up space charges increased due to X-ray flux. Note that the charges are not only distributed in the blank region, where there is no potential contour (Figs. 3(c)−(e)), but also throughout the bulk of the CdZnTe crystal. Moreover, the distribution is correlated directly with the density of space charges that may form a region as mentioned above.

In conclusion, the intensifying process of polarization at room temperature is investigated. We present a possible explanation on the process based on the dramatic changes in the electric potential with increasing photon flux. The reported results indicate that the build up space charges have affected the electric potential distribution deeply. At high flux irradiation, the rate of charge injection into the CdZnTe crystal is high enough that a significant net space charge accumulated in the bulk. It suggests that dramatic changes in electric potential due to increasing space charge in the crystal may be responsible for both the formation of polarization and the expansion of the space charges region. This result can contribute to the further understanding of the process of polarization in CdZnTe detectors.

This work was supported by the National Science Associated Foundation of China (No. 10876044) and the Fundamental Research Funds for the Central Universities (No. CDJXS11122219).

References

1. H. Zheng, A. Wang, L. Xu, K. Gao, and H. Ming, Chin. Opt. Lett. **8,** 248 (2010).
2. A. Ince-Cushman, J. E. Rice, M. Reinke, M. Greenwald, G. Wallace, R. Parker, C. Fiore, J. W. Hughes, P. Bonoli, S. Shiraiwa, A. Hubbard, S. Wolfe, I. H. Hutchinson, and E. Marmar, Phys. Rev. Lett. **102,** 035002 (2009).
3. R. Wang, W. Chen, C. Mao, J. Dong, and S. Fu, Chin. Opt. Lett. **7,** 156 (2009).
4. T. E. Schlesinger, J. E. Toney, H. Yoon, E. Y. Lee, B. A. Brunett, L. Franks, and R. B. James, Mater. Sci. Eng. **32,** 103 (2001).
5. G. Prekas, P. Sellin, P. Veeramani, A. Davies, A. Lohstroh, M. Ozsan, and M. Veale, Appl. Phys. **43,** 085102 (2010).
6. A. Bolotnikov, G. Camarda, G. Carini, Y. Cui, L. Li, and R. James, Nucl. Instrum. Meth. A **571,** 687 (2007).
7. S. Soldner, D. Bale, and C. Szeles, IEEE Trans. Nucl. Sci. **54,** 1723 (2007).
8. P. J. Sellin, G. Prekas, J. Franc, and R. Grill, Appl. Phys. Lett. **96,** 133509 (2010).
9. D. Bale, S. Soldner, and C. Szeles, Appl. Phys. Lett. **92,** 082101 (2008).
10. X. Wang, S. L. Xiao, L. Q. Zhang, Y. X. Chen, Y. L. Cao, M. Li, M. Shen, X. Cai, and J. Jiang, J. Optoelectron. Laser (in Chinese) **21,** 639 (2010).
11. D. S. Bale, Nucl. Instrum. Meth. A **614,** 453 (2010).
12. M. Li, S. Xiao, L. Zhang, Y. Cao, Y. Chen, M. Shen, and X. Wang, Chin. Phys. Lett. **27,** 070702 (2010).